Extracting dynamics from collision data. II. An application to $e+He$

X. C. Pan and A. Chakravorty
Department of Physics and The James Franck Institute, The University of Chicago, Chicago, Illinois 60637
(Received 21 December 1989)

The procedure of the preceding paper [Bohn and Fano, Phys. Rev. A **41**, 5953 (1990)] has been applied to extract dynamical parameters of the collision process $e(80\ \text{eV})+\text{He}(1\,^1S)\rightarrow e+\text{He}(2\,^1P)$. These parameters, free of the experimental geometry, have been unraveled from the experimental polarization data available and their roles in the excitation and the alignment of the target have been analyzed.

I. INTRODUCTION

The identification of dynamical information from experimental collision data has attracted extensive study, without arriving at an explicit solution.[1] These early studies focused on disentangling dynamical parameters from observables which are bilinear combinations of scattering matrix elements. Interferences among such matrix elements induced oscillations and slow convergence in the Fourier analysis of observables. An alternative, more straightforward, procedure which extracts the matrix elements directly from the observables measured in "complete" experiments has now been developed.[2]

The main purpose of this paper is to apply the procedure of Ref. 2 to the process

$$e(80\ \text{eV})+\text{He}(1\,^1S)\rightarrow e+\text{He}(2\,^1P)\ , \tag{1}$$

which has been widely studied in experiments providing a large set of polarization and cross-section data.[3] A set of dynamical parameters thus extracted will be reported here, with analysis and discussion of their roles in the process (1).

The unraveling of dynamical parameters has been approached in two different frames: (i) the conventional transition amplitudes[4] which are calculable directly by existing theory; (ii) the probability amplitudes defined in Ref. 3 which are essentially transition amplitudes scaled down by the square root of the differential cross section. Note that the experimental study of target polarization is generally carried out within frame (ii).

As discussed in Sec. II, forward scattering predominates in higher-energy collisions, whereby transition amplitudes and differential cross sections concentrate in a small range of scattering angles ($<30°$); their peaks spread out in the probability amplitudes which have smoother profiles throughout the angular range. Because of this smoothness, we will mainly unravel dynamical parameters in the frame (ii), but will also analyze them within frame (i).

A second purpose of this paper is to demonstrate the application of the concept, developed in Ref. 4, of sorting out the effect of long-range interactions which can be evaluated by the first-order Born approximation (FBA). The aggregate effect of weak long-range interactions between projectile and target contributes heavily to both the target alignment and the cross section. These long-range interactions involve numerous partial waves and hence a large set of dynamical parameters; their evaluation by FBA affords analytic compactness. Departures from the FBA evaluation, to be dealt with in this paper, will thus prove more tractable.

Section II reviews the theory for process (1). The transition amplitudes and the probability amplitudes are extracted from the experimental data; their FBA values are also evaluated separately in Sec. III. Results and analysis are presented in Sec. IV. Section V contains some final remarks and comments.

II. THEORY AND FORMULAS

The probability amplitude $\langle L_B M_B \mathbf{k}_f | a | L_A M_A \mathbf{k}_i \rangle$ introduced in Ref. 3 is related to the standard transition amplitude $\langle L_B M_B \mathbf{k}_f | T | L_A M_A \mathbf{k}_i \rangle$ by[3,4]

$$\langle L_B M_B \mathbf{k}_f | a | L_A M_A \mathbf{k}_i \rangle = \langle L_B M_B \mathbf{k}_f | T | L_A M_A \mathbf{k}_i \rangle \times \left[\frac{k_i}{k_f} \frac{d\sigma(\theta)}{d\Omega} \right]^{-1/2} , \tag{2}$$

where

$$\cos\theta = \hat{\mathbf{k}}_f \cdot \hat{\mathbf{k}}_i\ . \tag{2a}$$

Here $\mathbf{k}_f$ and $\mathbf{k}_i$ are the final and initial wave vectors of the projectile, (L_B, M_B) and (L_A, M_A) are the final and initial angular momentum quantum numbers of the target, and $d\sigma(\theta)/d\Omega$ is the differential cross section.

The transition operator T is proportional to the operator T' that satisfies the Lippman-Schrödinger equation

$$T' = V + V(E - H + i\epsilon)^{-1} T' \tag{2b}$$

through the dimensional and sign factors:[5]

$$T' = -\left[\frac{2m}{4\pi\hbar^2} \right] T\ . \tag{2c}$$

Here m is the reduced mass of the projectile and the target.

Containing all of the dynamical and the geometrical information of the collision process,

$\langle L_B M_B \mathbf{k}_f | a | L_A M_A \mathbf{k}_i \rangle$ pertains to the fractional probability of excitation from the initial state of the target to alternative final states, while $\langle L_B M_B \mathbf{k}_f | T | L_A M_A \mathbf{k}_i \rangle$ pertains instead to the actual cross section of excitation.

In process (1), $L_A = 0$ and $M_A = 0$ because of the spherical symmetry of the initial state of the target. Only the final state quantum numbers L_B and M_B of the target appear in both the probability amplitude $\langle L_B M_B \mathbf{k}_f | a | 00 \mathbf{k}_i \rangle$ and the transition amplitude $\langle L_B M_B \mathbf{k}_f | T | 00 \mathbf{k}_i \rangle$, which we will indicate as $a_{M_B}(\theta)$ and $T_{M_B}(\theta)$ for brevity, respectively.

The collisionally excited state of the He target in (1) is a coherent linear superposition of $|M_B\rangle$ components along the incidence axis:

$$|^1P_1\rangle = a_0|0\rangle + a_1|1\rangle + a_{-1}|-1\rangle \tag{3}$$

with $L_B = 1$. Here $a_{M_B}(\theta)$ indicates the probability amplitude of the magnetic substate $|M_B\rangle$ among the $2P$ states of He; extraction of the $a_{M_B}(\theta)$ from experiments to within a phase factor is described in Sec. III. We shall set this factor so that $a_0(\theta)$ is real. Here spin flips of the electron have been disregarded in view of the weak spin-orbit coupling. Symmetry under reflection with respect to the scattering plane requires $a_1 = -a_{-1}$.[6]

In an alternative form,[2] $a_{M_B}(\theta)$ is indicated in terms of dynamical parameters and of geometric factors (scattering angle and orbital quantum numbers of the projectile) by

$$\begin{aligned} a_{M_B}(\theta) = \sum_{l_a, l_b, m_b} & i^{l_a - l_b - 1} \left[\frac{2l_a + 1}{4\pi} \right]^{1/2} \\ & \times Y^*_{l_b m_b}(\theta, 0)(-1)^{l_b - m_b} \\ & \times \langle L_B M_B | l_a 0 l_b - m_b \rangle \\ & \times \langle L_B 0 | G | l_b \, l_a \rangle , \end{aligned} \tag{4}$$

which requires $m_b + M_B$ to vanish. The desired dynamical parameters G are then obtained by inverting Eqs. (4), as in Eq. (21) of Ref. 2,

$$\begin{aligned} \langle L_B 0 | G | l_b l_a \rangle = & \frac{2l_a + 1}{2L_B + 1} i^{l_b - l_a + 1} \left[\frac{2l_a + 1}{4\pi} \right]^{-1/2} \\ & \times \sum_{M_B} 2\pi \langle l_a 0 l_b M_B | L_B M_B \rangle (-1)^{l_b - M_B} \\ & \times \int_{-1}^{+1} d(\cos\theta) Y_{l_b m_b}(\theta, 0) a_{M_B}(\theta) . \end{aligned} \tag{5}$$

Equations (4) and (5) differ from (21) of Ref. 2 by including in G a factor i.

The null values of (L_A, M_A) for the initial state and the value $L_B = 1$ for the final state of the target state make it possible to reduce Eq. (5) to a very simple and instructive form,

$$\begin{aligned} \langle 1\,0 | G | l_a + 1 \; l_a \rangle = & \frac{4\pi^{3/2}}{[3(2l_a + 3)]^{1/2}} \\ & \times [(l_a + 1)^{1/2} A_0(l_a + 1) \\ & - (2l_a + 4)^{1/2} A_1(l_a + 1)] , \end{aligned} \tag{6}$$

$$\begin{aligned} \langle 1\,0 | G | l_a - 1 \; l_a \rangle = & \frac{4\pi^{3/2}}{[3(2l_a - 1)]^{1/2}} \\ & \times [\sqrt{l_a} A_0(l_a - 1) \\ & + (2l_a - 2)^{1/2} A_1(l_a - 1)] , \end{aligned} \tag{6'}$$

with

$$A_{M_B}(l_b) = \int_{-1}^{+1} d(\cos\theta) Y_{l_b - M_B}(\theta, 0) a_{M_B}(\theta) . \tag{7}$$

The parameter $\langle 1\,0 | G | l_a + 1 \; l_a \rangle$ is called unfavored and $\langle 1\,0 | G | l_a - 1 \; l_a \rangle$ favored as discussed below. Notice in Eqs. (6) that the value of A_0 is real and that the imaginary part of G depends on that of A_1, that is, on that of $a_1(\theta)$ averaged through the integration in Eq. (7). The physical roles of the imaginary parts of $a_{M_B}(\theta)$ and G will be discussed in Sec. IV.

Since the angular momentum quantum number l_a ranges to infinity, the sum $l_a + l_b$ is unrestricted, even though $|l_a - l_b|$ is restricted to $\leq L_B$ by the triangular condition on (l_a, l_b, L_B); a large set of dynamical parameters G identified by (l_a, l_b) is thus anticipated. The aggregate contribution of this set of small G values with large (l_a, l_b) remains finite. On the other hand, the small values of G with large (l_a, l_b) are adequately represented by the analytic Born formula.[4] Therefore we shall concentrate on the departure $G^R = G - G^B$ of each experimental value G from its FBA value G^B; the convergence of G^R with increasing (l_a, l_b) is readily tractable because of cancellation between G and G^B for high values of (l_a, l_b).

Although the theory and formulas have been developed above in the frame (ii) for probability amplitudes, a parallel development can be carried out in the frame (i) of transition amplitudes. An alternative set of dynamical parameters will be extracted from transition amplitudes according to Eq. (5), defined by

$$\begin{aligned} \langle L_B 0 | H | l_b l_a \rangle = & \left[\frac{2l_a + 1}{2L_B + 1} \right] i^{l_b - l_a + 1} \left[\frac{2l_a + 1}{4\pi} \right]^{-1/2} \\ & \times \sum_{M_B} 2\pi \langle l_b M_B l_a 0 | L_B M_B \rangle (-1)^{l_b + M_B} \\ & \times \int_{-1}^{+1} d(\cos\theta) Y_{l_b m_b}(\theta, 0) T_{M_B}(\theta) , \end{aligned} \tag{8}$$

with $T_{M_B}(\theta)$ standing for the T of (2).

Recall here that the definition (8) of H differs from the definition (5) of G by the replacement of $a_{M_B}(\theta)$ with $T_{M_B}(\theta)$ in accordance with (2). The transition amplitude $T_{M_B}(\theta)$ itself is related by (2c) to the solution of the

Lippman-Schrödinger equation (2b) for He excitation to the magnetic sublevel M_B.

As in the treatment of the parameter G, the deviation of the experimental value of H from its FBA value will be dealt with here and indicated by H^R.

III. DATA FITTING

The experimental polarization data available for process (1) are familiarly translated into a pair of real parameters. Conventionally two different but interconvertible parametrizations are utilized: $\{L_\perp(\theta),\gamma(\theta)\}$ or $\{\lambda(\theta),\chi(\theta)\}$.[3] $L_\perp(\theta)$ indicates the expectation value of the angular momentum component of the excited target perpendicular to the scattering plane and $\gamma(\theta)$ represents the alignment angle of the excited charge cloud relative to the incidence direction. In the alternative parametrization, $\lambda(\theta)$ is the fractional excitation probability of the $M_B=0$ state and $\chi(\theta)$ stands for the phase difference of $a_0(\theta)$ and $a_1(\theta)$.[3]

From either of these two sets of parameters, the probability amplitudes $a_M(\theta)$ can be determined to within a phase factor, which has been set by letting $a_0(\theta)$ be real,

$$a_0(\theta)=\tfrac{1}{2}\{1+[1-L_\perp^2(\theta)]^{1/2}\cos 2\gamma(\theta)\} \tag{9}$$

and

$$\mathrm{Re}[a_1(\theta)]=-\frac{[1-L_\perp^2(\theta)]^{1/2}\sin 2\gamma(\theta)}{2a_0(\theta)}\ ;$$

$$\mathrm{Im}[a_1(\theta)]=-\frac{L_\perp(\theta)}{\sqrt{8}a_0(\theta)}\ . \tag{9'}$$

Alternatively,

$$a_0(\theta)=\sqrt{\lambda(\theta)} \tag{10}$$

and

$$\mathrm{Re}[a_1(\theta)]=\left[\frac{1-\lambda(\theta)}{2}\right]^{1/2}\cos\chi(\theta)\ ;$$

$$\mathrm{Im}[a_1(\theta)]=\left[\frac{1-\lambda(\theta)}{2}\right]^{1/2}\sin\chi(\theta)\ . \tag{10'}$$

Two procedures, namely, χ^2 fitting and interpolation-extrapolation have been applied separately to the polarization data available from the experiments[7–9] in order to produce smooth curves for $\{L_\perp(\theta),\gamma(\theta)\}$ and, alternatively, for $\{\chi(\theta),\lambda(\theta)\}$ over the whole range of the scattering angles. Two difficulties emerged in implementing these procedures.

(1) There remain some discrepancies among the polarization data reported by different authors. For example, the values of $\{\lambda(\theta),\chi(\theta)\}$ reported in Ref. 7 differ from those of Refs. 8 and 9 by as much as 30–40 % in the angular range 70°–110°. This introduces an uncertainty of 20% in the probability amplitudes for that range.

(2) Data lack for large scattering angles (130°–180°) as seen in Fig. 3.1.3h and Fig. 3.1.3i of Ref. 3.

We resolved the first issue by using mainly data from Refs. 8 and 9 in the angular range 70°–110°. This seems reasonable since these two different sets of data agree fairly well with each other. In addition, the reported error bars were much smaller for these sets of data than for those of Ref. 7. The extrapolation to large scattering angles, however, remains ambiguous to about 10%. While this ambiguity introduces an uncertainty in the calculation of $a_{M_B}(\theta)$ in Eqs. (9) and (9′) or Eqs. (10) and (10′), no indication exists of significant error in the general trend of $a_{M_B}(\theta)$.

Fits for the two alternative parametrizations were carried out independently by the two authors. About 35 points of experimental data were used in χ^2 fitting, with resulting χ^2 values of around 50.

The curves for the probability amplitudes $a_{M_B}(\theta)$ were then calculated from the fitted parameters $(L_\perp(\theta),\gamma(\theta))$ or $(\chi(\theta),\lambda(\theta))$ by use of Eqs. (9) and (10). Figures 1(a)–1(c) show the curves of $a_{M_B}(\theta)$. The corresponding FBA values $a^B_{M_B}(\theta)$, on the other hand, are evaluated through the FBA value $\gamma^B(\theta)$ which is related analytically to the momentum transfer in the collision,

$$\gamma^B(\theta)=\frac{\sin\theta}{\cos\theta-x^{-1}}\ . \tag{11}$$

Here θ indicates the scattering angle and $x=k_f/k_i$ is the ratio of the final and the initial momenta of the projectile. The expectation value $L_\perp^B(\theta)$ vanishes in FBA because of cylindrical symmetry of the collision about the wave vector $\mathbf{k}_i-\mathbf{k}_f$. The evaluated departures $a^R_{M_B}=a_{M_B}-a^B_{M_B}$ are shown in Figs. 1(a)–1(c), respectively, for process (1).

Combining the differential cross-section data represented in Ref. 3 and the data of $a_{M_B}(\theta)$ from Eqs. (3), the experimental transition amplitude is obtained at each scattering angle. The corresponding FBA differential cross section is expressed by[10]

$$\frac{d\sigma^B(\theta)}{d\Omega}=\frac{4a_0^2}{(k_ia_0)^4}\frac{xf(\theta)}{(1-x^2)(1+x^2-2x\cos\theta)}\ , \tag{12}$$

where a_0 is the Bohr radius and $f(\theta)$ indicates the generalized oscillator strength of He. Here a semitheoretical formula[11]

$$f(\theta)=\frac{0.2762}{(1+y)^6}\left[1+\frac{0.87y}{1+y}\right] \tag{13}$$

with

$$y=\frac{(k_ia_0)^2}{3.391}(1+x^2-2x\cos\theta) \tag{13'}$$

has been applied to determine the function $f(\theta)$ to be entered in Eq. (12).

The FBA values of transition amplitudes have been evaluated from the calculated values of $d\sigma(\theta)/d\Omega$ and the $a^B_{M_B}(\theta)$ in Figs. 1(a)–1(c). Figure 2 gives the differences $T^R_{M_B}$ between the experimental and FBA values of transition amplitudes. Overestimates inherent in the FBA values at small scattering angles cause the transition amplitude residue $T^R_{M_B}$ to be negative. It is noticed that

the concentration of transition amplitudes in the small range of scattering angles ($<30°$) (see Fig. 2) spreads out in the probability amplitudes (see Fig. 1).

IV. RESULTS AND ANALYSIS

A. The probability amplitudes $a_{M_B}(\theta)$

The fitted values of $a_{M_B}(\theta)$ from experimental polarization data are shown in Fig. 1. Some features of these

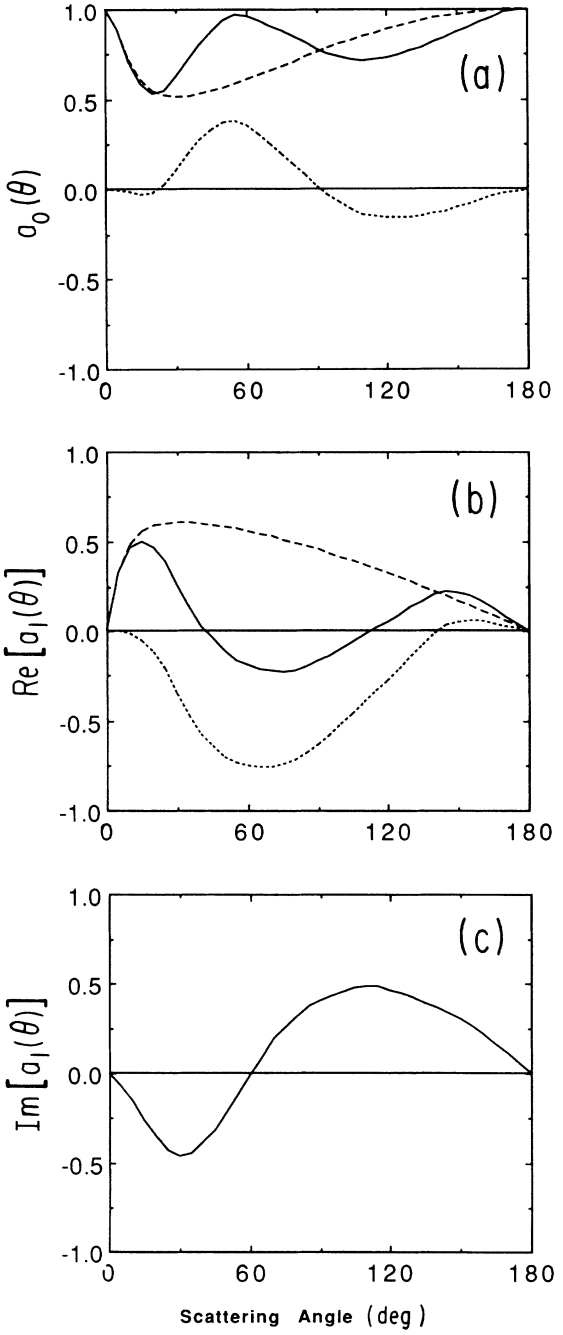

FIG. 1. Values of probability amplitudes. (a) $a_0(\theta)$, —; $a_0^B(\theta)$, — — —; $a_0^R(\theta)$, - - - . (b) Re$[a_1(\theta)]$, —; Re$[a_1^B(\theta)]$, — — —; Re$[a_1^R(\theta)]$, - - - . (c) Im$[a_1(\theta)]$ = Im$[a_1^R(\theta)]$, —.

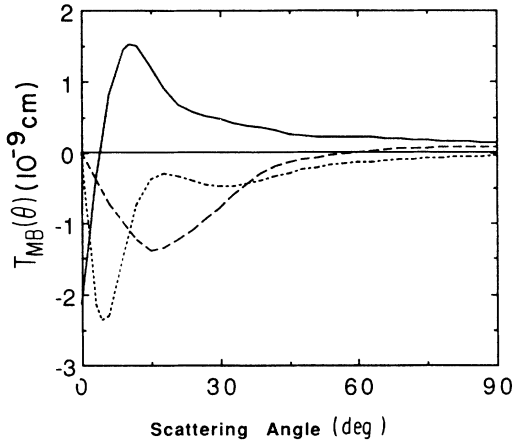

FIG. 2. Transition amplitude residues (10^{-9} cm). $T_0^R(\theta)$, —; Re$[T_1^R(\theta)]$, — — —; Im$[T_1^R(\theta)]$, - - - .

curves are readily understood. At the extremely forward and backward scattering angles ($\theta \to 0°$ and 180°), we have $a_0(\theta) \to 1$ and $a_1(\theta) \to 0$; only the magnetic substate $|0\rangle$ of the He $2P$ state is excited because the momentum transfer along the z axis contributes no angular momentum in that direction. Since forward scattering is favored, most $a_{M_B}(\theta)$ values lie in the range $\theta < 90°$; nevertheless, the probability amplitudes $a_{M_B}(\theta)$ are indeed widely spread out as compared with the concentration of the corresponding transition amplitudes $T_{M_B}(\theta)$ ($<30°$) (see Fig. 2).

The actual dependence of $a_0(\theta)$ on the scattering angle seems obscure, but can be understood with the help of the curves in Figs. 1(a)–1(c) of $a_0(\theta)$ and $a_1(\theta)$. First of all, the Im$[a_1(\theta)]$ originates from the second term of the Lippman-Schwinger Eq. (2b) as a generalized Hilbert transform of the Re$[a_1(\theta)]$. Accordingly, Im$[a_1(\theta)]$ is roughly proportional to the derivative of $|\text{Re}[a_1(\theta)]|$ which peaks at $\sim 70°$; this is why Im$[a_1(\theta)]$ goes through a zero. On the other hand, $a_1^B(\theta)$ originates from the first term of (2b) and remains real. A second feature of Fig. 1 stems from the normalization relation among $a_0(\theta)$, Im$[a_1(\theta)]$, and Re$[a_1(\theta)]$, $|a_0|^2 + 2|\text{Re}(a_1)|^2 + 2|\text{Im}(a_1)|^2 = 1$. It requires $a_0(\theta)$ to approach unity where *both* $|\text{Re}[a_1(\theta)]|^2$ and $|\text{Im}[a_1(\theta)]|^2$ are small, as apparent from Figs. 1(b) and 1(c), respectively.

The imaginary part of $a_1(\theta)$ plays an important role in process (1), by setting the sign of the target angular momentum $L_\perp(\theta)$, according to (9′). Note here that Im$[a_1(\theta)]$, and hence $L_\perp(\theta)$, vanish unless the excited charge cloud astride the scattering plane loses the cylindrical symmetry about the momentum transfer $\mathbf{k}_i - \mathbf{k}_f$ which is characteristic of the FBA.

The shortage of measurements at small and particularly at large scattering angles makes the fitting of $a_{M_B}(\theta)$ in these ranges ambiguous. This ambiguity extends of course to the values of $a_{M_B}^R(\theta)$. For instance, Re$[a_1(\theta)]$ becomes larger than its FBA value after $\theta \sim 130°$, in Fig. 1(b), but this feature needs verification because it depends

on extrapolation of the probability amplitudes extracted from scarce experimental data. Although the values of $a_{M_B}(\theta)$ remain ambiguous at small and large scattering angles, the smallness of these values and the plots of $a_{M_B}(\theta)$ in Fig. 1 suggest that it should have a minor effect on the dynamical parameters $\langle L_B 0|G^R|l_b l_a\rangle$, except possibly for large values of the orbital momenta (l_a,l_b). The same ambiguity, on the other hand, has a lesser effect on the transition amplitudes $T_{M_B}(\theta)$ shown in Fig. 2, whose backscattering values are negligible as compared to their forward peaks. Its influence on the dynamical parameters H^R will be similarly reduced.

B. The dynamical parameters

We focus here on the values of the "residue" parameters $\langle L_B 0|G^R|l_b l_a\rangle$, which are evaluated by Eq. (5) with the residue $a^R_{M_B}(\theta)$ in place of $a_{M_B}(\theta)$. A main issue concerns the convergence of the G^R as (l_b,l_a) increase; specifically we look into their convergence with increasing l_a—i.e., with the total angular momentum—since $l_b=l_a\pm1$. This convergence is illustrated in Fig. 3 by plotting the moduli $|G^R|$ rather than their real or imaginary parts whose signs may alternate.

The separate plots of $|G^R|$ for $l_b=l_a\mp1$ decay rapidly as l_a increases, falling to $\sim6\%$ of their peak values, as expected. We attribute their jagged behavior at large l_a (by $\leq1\%$ of the peak values) to inaccuracies of measurement and of curve fitting. The nearly linear decay of the $|G^R|$ for $l_a\leq6$, on the logarithmic scale, implies an approximate law

$$|G^R|\propto e^{l_a/l_0}, \tag{14}$$

with $l_0\sim1.5$. The parameter l_0 represents the number of partial waves of the incident electron that are expected to penetrate the target atom; the exponential law (14) may be viewed as representing the target's profile. The fitted value $l_0\sim1.5$ appears plausible considering that (a) the projectile's kinetic energy exceeds that of the target electrons by a factor of ~3, implying $l_0\sim\sqrt{3}$, and (b) the projectile's penetration is opposed by exchange forces but favored by the nuclear attraction.

Figure 3 also displays FBA values $|G^B|$, which decay less sharply than exponentials. Indeed the analytical treatment of FBA in Ref. 4 indicates a convergence of scattering amplitudes proportional to a second kind Legendre function of l_a.

A parallel evaluation of the parameters $|H^R|$, through Eq. (8), has documented their much slower convergence resulting from the sharp peaking of $T^R_{M_B}(\theta)$ at small scattering angles. Typically the value of $\langle L_B 0|H^R|l_a\pm1\ l_a\rangle$ for $l_a=10$ still amounts to $\sim15\%$ of its peak value.

Displayed in Fig. 3 is the influence of the propensity rule that favors the transitions $l_a\to l_b=l_a-1$ over those with $l_a\to l_b=l_a+1$. The qualitative interpretation of this rule in Ref. 12 suggests that it might apply mainly to large values of l_a with lesser influence in the lowest range of l_a. Figure 3 shows its violation at $l_a\leq1$.

Figure 4 shows, in contrast to $|G^R|$, the real and imagi-

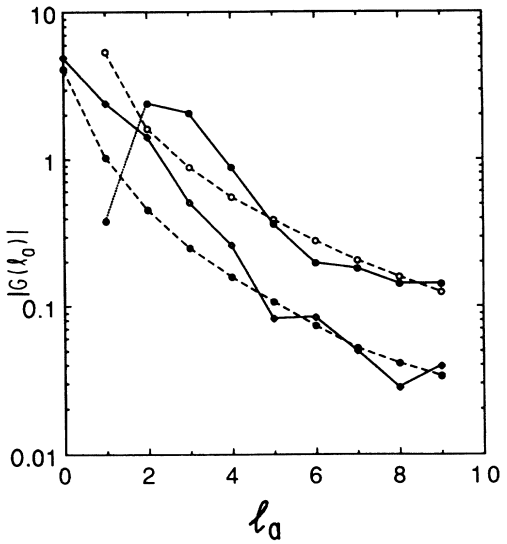

FIG. 3. Dynamical parameters. $|G^R|$: favored $(l_b=l_a-1)$, -●-; unfavored $(l_b=l_a+1)$, -□-. $|G^B|$: favored $(l_b=l_a-1)$, - - ○ - -; unfavored $(l_b=l_a+1)$, - -●- -.

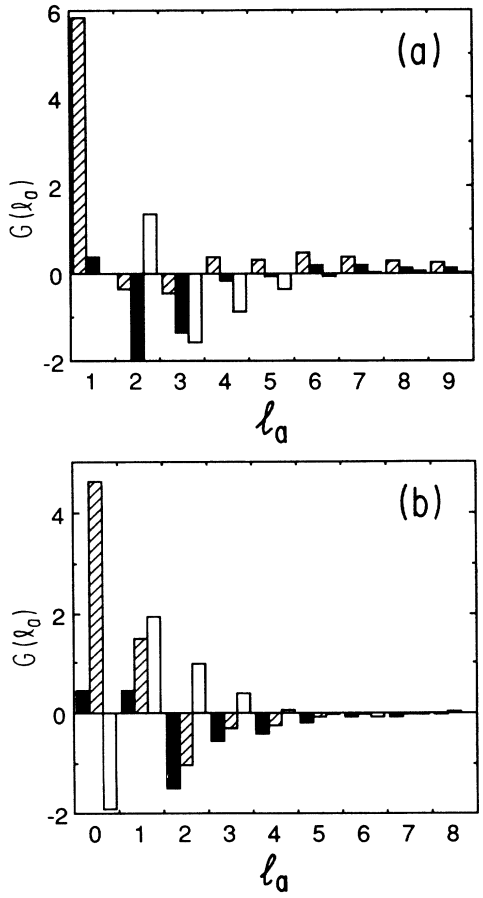

FIG. 4. The values of the real and imaginary parts of the dynamical parameters (a) favored $(l_b=l_a-1)$; (b) unfavored $(l_b=l_a+1)$. Re(G), ▨ ; Re(G^R), ■; Im(G)=Im(G^R), □.

nary parts of G^R as functions of l_a. Their convergence at large l_a is partly obscured by sign reversals, as expected. Nevertheless, the sign reversals in Fig. 4 are readily understood. According to Eqs. (6) and (6'), the imaginary parts of the dynamical parameters G are totally determined by those of the probability amplitudes $a_1(\theta)$ which depend on the sign of the perpendicular component $L_\perp(\theta)$ of the target's angular momentum. With $l_a=0$, only the unfavored component of G [Eq. (6)] exists because l_b can only be 1. The combination of $Y_{1-1}(\theta,0)\propto\sin\theta$ and $\mathrm{Im}[a_1(\theta)]$ in Eq. (7) makes $\mathrm{Im}[A_1(1)]$ positive and consequently the imaginary part of $\langle 10|G|10\rangle$ negative because of the minus sign in front of $A_1(1)$ in Eq. (6). For $l_a=1$, the imaginary part of the favored component of G has null value because the factor $(2l_a-2)^{1/2}$ vanishes in Eq. (6'). In the corresponding unfavored component of G we have $l_b=2$ and $Y_{2-1}(\theta,0)\propto\sin2\theta$ and the integral $A_1(2)$ over the scattering angle in Eq. (7) becomes negative. The minus sign preceding $A_1(2)$ in Eq. (6) makes the imaginary part of the unfavored component of G positive in contrast to its value for $l_a=0$. Similarly, the sign reversals for higher l_a and for the real part of the dynamical parameters in Fig. 4 may be explained.

V. FINAL COMMENTS

Dynamical parameters G and H have been evaluated from the target orientations and alignments measured for process (1). These parameters are independent of the experimental geometry, as intended, but the connection of their magnitudes and signs to the observed data has been traced in Sec. IV.

The FBA contribution to these parameters—indicated by G^B (or H^B) and adequate for large orbital momenta—has been provided and analyzed by the procedure of Ref. 4. The parameter residues $G^R=G-G^B$, significant for low momenta only, can be expressed in terms of multichannel quantum defect theory (Refs. 13 and 14) eigenphases and eigenvectors accessible to *ab initio* R-matrix calculations,[15] whose prototype is currently in progress. A full eventual interpretation of experimental data remains to be traced through such calculation of the G^R.

We have used the dynamical parameters $G^R=G-G^B$ with $l_a\le 11$ to reconstruct $a_0(\theta)$. The $a_0^R(\theta)$ thus reconstructed is indistinguishable from the curve $a_0^R(\theta)$ in Fig. 1(a) except for an $\sim 2\%$ difference at $\theta\sim 0°$. This procedure has been tested further by multiplying the $a_0(\theta)$ thus reconstructed with the $\mathrm{Im}[a_1(\theta)]$ from Fig. 1(c) to yield the plot of $L_\perp(\theta)$ in Fig. 5, compared there with experimental values. The figure also shows the $L_\perp(\theta)$ reconstructed using only G^R values with $l_a\le 5$.

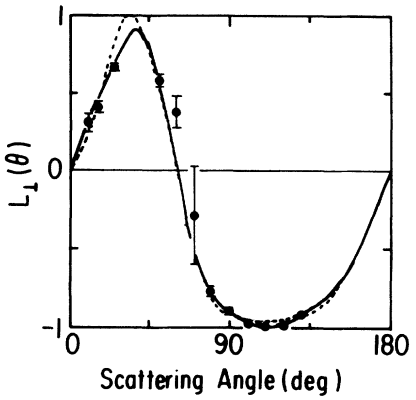

FIG. 5. The values of $L_\perp(\theta)$ reconstructed with the dynamical parameters G^R. The solid line is obtained with $l_a\le 11$ and the dashed line with $l_a\le 5$. ● are the experimental data of $L_\perp(\theta)$ from Ref. 9.

The present study of process (1) has been confined to collisions at 80 eV, the only example for which available data appeared adequate. Its extension to other energies and materials, including the targets with nonspherical symmetry treated by Ref. 2, remains open. The acquisition of the required data through "complete" experiments presents, however, a nontrivial challenge.

ACKNOWLEDGMENTS

We are indebted to Professor U. Fano for his continued guidance, insightful advice, and great help in the preparation of the manuscript. We also benefited from communication with Dr. Nils Andersen. This work has been supported by the National Science Foundation Grant No. PHY86-10129.

[1]C. W. Lee *et al.*, Phys. Rev. A **33**, 921 (1986) (paper I); **34**, 959 (1986) (paper II); **36**, 66 (1987) (paper III); **36**, 74 (1987) (paper IV); **39**, 554 (1989) (paper V).

[2]J. Bohn and U. Fano, preceding paper, Phys. Rev. A **41**, 5953 (1990).

[3]N. Andersen, J. W. Gallagher, and I. V. Hertel, Phys. Rep. **165**, 1 (1988).

[4]X. Pan and U. Fano, Phys. Rev. A **39**, 4502 (1989).

[5]L. S. Rodberg and R. M. Thaler, *Introduction to the Quantum Theory of Scattering* (Academic, New York, 1967), p. 172.

[6]K. Blum and H. Kleinpoppen, Phys. Rep. **52**, 205 (1979).

[7]N. C. Steph and D. E. Golden, Phys. Rev. A **21**, 1848 (1980).

[8]M. T. Hollywood, A. Crowe, and J. F. Williams, J. Phys. B **12**, 819 (1979).

[9]M. Eminyan *et al.*, J. Phys. B **7**, 1519 (1974); **13**, 3009 (1980).

[10]M. Inokuti, Rev. Mod. Phys. **43**, 297 (1971).

[11]E. N. Lassettre, A. Skerbele, and M. A. Dillon, J. Chem. Phys. **50**, 1821 (1969).

[12]U. Fano, Phys. Rev. A **32**, 617 (1985).

[13]M. J. Seaton, Rep. Prog. Phys. **46**, 1 (1983).

[14]C. H. Greene, A. R. P. Rau, and U. Fano, Phys. Rev. A **26**, 2441 (1982).

[15]C. H. Greene, Phys. Rev. A **32**, 1880 (1985).